Fractional order harmonic disturbance observer control for three-phase LCL-type inverter☆

Jinmu Lai [a,b], Xin Yin [c,*], Xianggen Yin [b], Lin Jiang [c]

[a] School of Electrical Engineering, Zhengzhou University, Zhengzhou 450001, China
[b] State Key Laboratory of Advanced Electromagnetic Engineering and Technology, and School of Electrical and Electronic Engineering, Huazhong University of Science and Technology, Wuhan 430074, China
[c] Department of Electrical Engineering and Electronics, University of Liverpool, Liverpool L69 3GJ, United Kingdom

ARTICLE INFO

Keywords:
LCL-type three-phase inverter
Periodic disturbances
Frequency deviation
Fractional order harmonic disturbance observer

ABSTRACT

The quality of output current of LCL-type voltage source inverter (VSI) is degraded by the grid voltage distortion, the dead time effect, and the parameter mismatches. This paper proposes a novel fractional order harmonic disturbance observer-based control (FOHDO) for the three-phase LCL-type inverter to suppress all the dc- and ac-component periodic disturbances. Firstly, a harmonic disturbance observer based control for LCL-type inverter is proposed with the internal model knowledge of the periodic disturbances signals. Subsequently, the FOHDO based on Lagrange interpolating polynomial fractional order delay approximation is put forward to enhance the adaptability of the grid frequency. Then, the stability and robustness performance of the proposed FOHDO for LCL-type inverter are evaluated, which also involves a detailed parameter design process. Finally, the effectiveness and performance of the proposed FOHDO method are verified by both experimental and simulation results.

1. Introduction

Voltage source inverter is widely used in distributed power generation and power quality control and other fields because of its simple structure and versatile control (Blaabjerg et al., 2006, 2004). A suitable L-type or LCL-type filter can be used in the inverter output to eliminate switching harmonics in grid-connected current due to pulse width modulation(PWM). Compared to L-type filter, LCL-type filter is considered to be a preferred choice for its higher attenuating ability to improve the power quality with smaller size and cost-effective (Li, Sun et al., 2013; Ruan, 2018), while more complex control and a more sophisticated design (Peña-Alzola et al., 2013). Due to high order and coupling dynamic of LCL filter (Li, Sun et al., 2013; Osório et al., 2019; Ruan, 2018), the quality of output current of LCL-type inverter is degraded by the multi-frequencies ac-component periodic disturbances, including the grid voltage distortion, the dead time effect, and the parameter mismatches. Therefore, the well-designed current controller becomes a crucial part of the LCL-type inverter system.

In general, the ac-component periodic disturbances induced by a dead time effect lead to sinusoidal harmonic distortions of the inverter output voltages, and then propagate to the output currents (Jiao et al., 2019). Dead time is the main source of distortion, even a short dead time less than 1% of the PWM period can cause a large distortion level (Chierchie et al., 2019). Various strategies have been suggested to resolve the dead-time effect, often on the basis of dead time elimination (Chen & Peng, 2008; Wang et al., 2011) and dead time compensation methods (Blaabjerg et al., 1997; Tang & Akin, 2017). These methods encounter problems like ripple current immunity, dynamic performance, or complexity for the LCL-type inverter.

The ac-component periodic disturbances caused by the grid voltage distortion harmonics also affect the output current quality of the LCL-type inverter (Erika Twining & Holmes, 2003). Grid voltage distortion may occur in the actual distribution grid, especially in some remote areas. In Li, Ruan et al. (2013) and Ruan (2018), the full-feedforward of grid voltages for three-phase LCL-type inverter in synchronous dq-frame was proposed and investigated to reduce the output current harmonics caused by the grid voltage. However, this scheme raises concern about the complexity of the controller. In addition, the uncertainties of the LCL filter parameters degrade the control performance. Due to the complex high-order LCL filter, the analysis of feedforward method for a three-phase LCL-type inverter in synchronous dq-frame is relatively limited. Therefore, for the three-phase LCL-type inverter in synchronous dq-frame, an efficient and straightforward way for suppressing the output current harmonics induced by the grid voltage distortion is important.

The grid voltage distortion, the dead-time effect, the uncertainties of the parameters and other factors can be aggregated into the disturbances. Repetitive controller (RC) (Trivedi & Singh, 2017; Yang et al., 2018) is provided for rejecting periodic disturbances due to the introduction of high gains at interested harmonic frequencies, and has been widely used in PWM inverters. The transient response of single RC is poor, and the PI with RC is more popular due to its fast transient response. However, there exists control coupling between two regulators in the feedback loop, which causes current distortion during step transient response (Zhang et al., 2014). Until now, the output current distortion problem with RC during transient response remains challenging work that has not yet been reported.

Recently, many different advanced control strategies have been proposed for the nonlinear systems with high-precision, fast-response and disturbances suppression, i.e., sliding mode control (Sun & Ma, 2017; Yin et al., 2019), fuzzy adaptive finite-time control (Sun, Liu et al., 2020; Sun, Qiu et al., 2020; Sun et al., 2019), model predictive control (Wang et al., 2020), and disturbance observer based control (DOB) (Chen et al., 2016; Jiang You & Ghasemi, 2018). In general, DOB is an effective approach to estimate and compensate the disturbances. The DOB method performs well to eliminate the parameter and model uncertainties for L-type inverter in dq-frame (Errouissi & Al-Durra, 2018, 2019). As reported in Errouissi and Al-Durra (2018), the feedback linearization (FBL) technique with a DOB-based control was employed for an LCL grid-tied inverter to overcome model uncertainty and external disturbances. The authors in Liu et al. (2019) explored an adaptive PID with DOB for LCL-type grid-connected inverter. Beneficial from DOB, the steady-state and transient performance is increased. However, the grid voltage distortion could greatly deteriorate the conventional DOB performance, showing the evidence of weak ac-component periodic disturbances suppression ability of the conventional DOB. The output current distortion is attenuated by a group of resonant regulators in parallel with PID, which raises concerns about the reliability and stability of the controller. Therefore, further research and analysis for the LCL-type inverter are required to investigate the ability of suppression for the ac-component periodic disturbances. A periodic adaptive disturbance observer was proposed in Cho et al. (2015) to attenuate periodic disturbances for permanent magnet linear synchronous motors. However, a typical DOB is only used for the initial time period. In Elkayam et al. (2019), disturbance observer incorporates with multi-resonant terms to enhance rejection of periodic uncertainties and disturbances. In Chen and Tomizuka (2014) and Wu and Ye (2018), internal model-based disturbance observers were proposed to estimate the disturbance both in the low frequency region and at harmonic frequencies. Note that the time delay element f_s/f_1 (f_s is sampling frequency and f_1 is fundamental frequency) is located at the feedback loop, which causes current distortion during step transient response (Zhang et al., 2014). Moreover, the bandwidth of the periodic frequencies is narrow and therefore sensitive to the grid frequency variations, which degrades periodic suppression ability. And, the nominal stability is affected by the resonant characteristic of LCL filter. Therefore, it is similar to an RC rather than a DOB. In Muramatsu and Katsura (2018), a novel adaptive notch filter (ANF) periodic disturbance observer was proposed for frequency-varying periodic disturbance suppression. The adaptive algorithm raises concerns about the complexity of the control design. Moreover, the time-delay element f_s/f_1 may be fractional and is neglected in this paper. The fractional order part induced by frequency variations significantly affects harmonic suppression performance. It was found that the fractional order controller can improve the robustness and performance of the control system (Sun & Ma, 2017; Sun et al., 2018). However, as far as we know, few works applying the fractional order to DOB approach have been reported in the literature.

Summing up, although the DOB and PI–RC are widely accepted in terms of the suppression of the disturbances in inverters, there are several drawbacks or open issues associated with it:

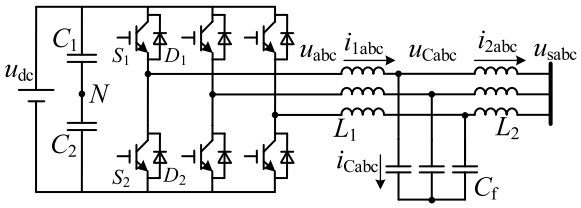

Fig. 1. Three-phase three-wire LCL-type inverter.

(i) The conventional DOB shows weak ac-component periodic disturbances suppression ability. Thus, although the DOB can achieve a dc-component disturbance suppression and fast transient response, the low-order ac-component periodic disturbances caused by grid voltage distortion and dead time effect can deteriorate the DOB performance.

(ii) The main drawback of the PI–RC is that it does not provide a fast transient response and there exists control coupling between two regulators in the feedback loop. As a consequence, the transient response is poor and the output current is distorted during step transient response.

This paper proposes a new control strategy named fractional order harmonic disturbance observer (FOHDO) for three-phase LCL-type inverter, which eliminates the output current harmonics caused by dc- and ac-component periodic disturbances and improves transient performance. In this paper, in order to improve DOB's ac-component periodic disturbances suppression ability, an infinite impulse response (IIR) (Karaboga, 2009) filter design technique, which achieves infinite loop gain at harmonic frequencies, is proposed that an internal model of ac-component disturbances signals is embedded in the DOB feedforward loop to estimate the periodic disturbances correctly. Different from the feedback loop of the PI–RC method, the proposed FOHDO is located at the feedforward loop and decoupled with feedback PI regulator. In addition, an improved FOHDO based on Lagrange interpolating polynomial finite-impulse-response (FIR) fractional order approximation (Yang et al., 2015; Zou et al., 2014) is proposed to improve HDO grid frequency adaptability. In conclusion, the originality and major contributions to the existing work are summarized as follows.

(i) Firstly, a novel harmonic disturbance observer-based control (HDO) is proposed for the three-phase LCL-type inverter to effectively eliminate all the multi frequencies periodic disturbances and significantly improve the output current quality.

(ii) We also propose a fractional order HDO (FOHDO) strategy at a fixed sampling rate to deal with any periodic disturbances of variable grid frequency, where a Lagrange-interpolation-based fractional order filter is used to approximate fractional order delay.

(iii) Moreover, the stability, robustness analysis and the detailed parameters design guideline of the proposed FOHDO for LCL-type inverters are given. Prototype experiment and on-field results of LCL-type inverter are also presented to verify the proposed FOHDO control.

2. Three-phase LCL-type inverter system modeling

The structure of three-phase LCL-type inverter system is shown in Fig. 1, which consists of three-phase two-level converter, the inverter-side inductor L_1, the grid-side inductor L_2, the filter capacitor C_f and the dc-link capacitor. u_{sabc} is the voltage at the point of common coupling, u_{abc} is the voltage at inverter side, u_{Cabc} is the voltage at filter capacitor, and u_{dc} is the dc-link voltage. i_{1abc}, i_{2abc} and i_{Cabc} are the currents at inverter-side, grid-side and filter capacitor, respectively. f_s is the sampling frequency. f_{sw} is the switching frequency.

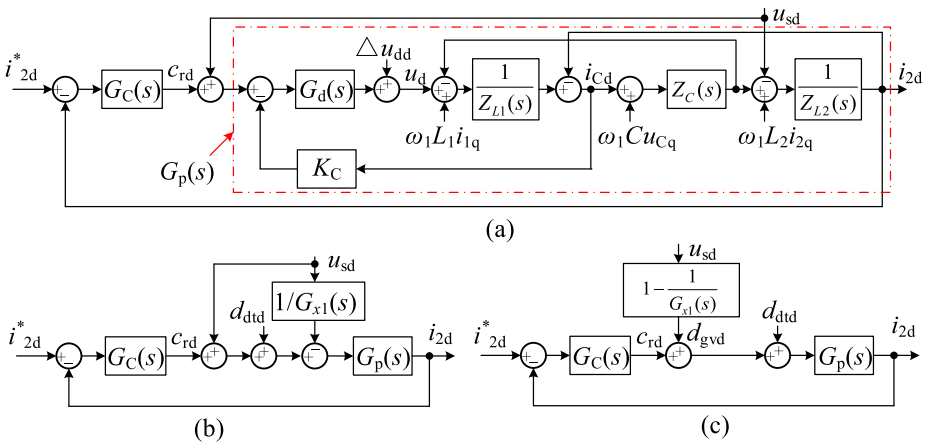

Fig. 2. Dual-current feedback with grid voltage feed forward control strategy in d-axis: (a) Detailed block diagram the dual-loop control strategy; (b) Equivalent transformation block diagram of the dual-loop control strategy; (c) Equivalent block diagram of Fig. 2(b).

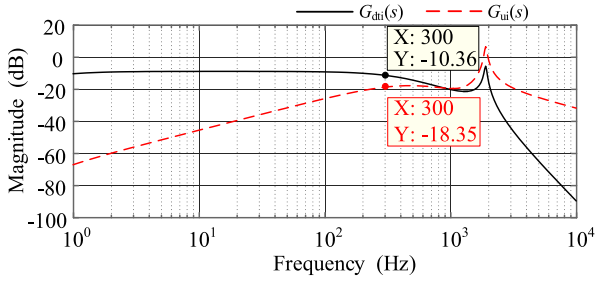

Fig. 3. Bode plot of $G_{dti}(s)$ and $G_{ui}(s)$ for LCL-type inverter with PI controller.

Assume that the coupling effects between dq-axis are considered as coupling disturbance. The dual-loop current feedback with the grid voltage direct feedforward method in d-axis is shown in Fig. 2 (Ruan, 2018), where $G_c(s) = K_p + K_i/s$ is the current loop regulator, K_c is the capacitor current feedback active damping (Pan et al., 2014), $G_d(s) = e^{-1.5sT_s} \approx 1/(1.5T_s s+1)$ is the time delay of the inverter system. w_1 is the grid angular frequency. $Z_{L1}(s) = sL_1$, $Z_C(s) = 1/(sC)$ and $Z_{L2}(s) = sL_2$ are the inverter-side inductance, filtering capacitance and grid-side inductance of LCL filter respectively.

Take d-axis as an example. According to Fig. 2, the equivalent plant $G_p(s)$ of the LCL filter with considering the active damping K_c and the time delay $G_d(s)$ is obtained as

$$G_p(s) = \frac{i_{2d}(s)}{c_r(s)} = \frac{G_d}{s^3 L_1 L_2 C + s^2 L_2 C K_c G_d + s(L_1 + L_2)} \tag{1}$$

It can be known from the amplitude–frequency characteristic of the equivalent transfer function $G_p(s)$ that the introduction of active damping can not only effectively suppress the resonance peak of LCL, but also retain the high low-frequency gain and high-frequency harmonic suppression capability of the LCL filter.

Moving the grid voltage $u_{sd}(s)$ to the input of $G_p(s)$, Fig. 2(a) can be equivalently transformed into Fig. 2(b), where $G_{x1}(s) = G_d(s)Z_C(s)/(Z_{L1}(s) + Z_C(s) + K_c G_d(s))$. Fig. 2(b) can be further depicted as shown in Fig. 2(c) by merging the grid voltage at the grid voltage feedforward node. Then, the grid voltage disturbance in the d-axis can be expressed as

$$d_{gvd}(s) = (1 - \frac{1}{G_{x1}(s)})u_{sd}(s) \tag{2}$$

Due to high order and complex coupling dynamic of LCL in dq-frame, the performance of the injected grid current is affected by the grid voltage disturbances. Furthermore, the closed-loop transfer function from the grid voltage $u_{sd}(s)$ to the grid-side current $i_{2d}(s)$ in d-axis can be obtained as

$$G_{ui}(s) = -\frac{s^2 L_1 C + sCK_c G_d + 1 - G_d}{s^3 L_1 L_2 C + s^2 L_2 C K_c G_d + s(L_1 + L_2) + G_c G_d} \tag{3}$$

In addition, the ac-component periodic disturbances induced by a dead time effect lead to sinusoidal harmonic distortions of the inverter output voltages, and then propagate to the output currents. During the dead time t_d period, the average error voltage Δu_{an} introduced by the dead-time effect t_d can be expressed in Fourier form (Jiao et al., 2019):

$$\Delta u_{an} = \frac{4Nt_d}{\pi T_s} u_{dc} \sum_{n=1}^{\infty} \frac{1}{n} \sin n\omega t \tag{4}$$

Due to the LCL filter is designed to filter the switching frequency harmonics, the low order harmonics introduced by the error voltage cannot be effectively attenuated, thus causing serious waveform distortion to the output voltage. When the dead time t_d is increased, the amplitude of each harmonic voltage in (4) also increases, which may increase the distortion of the output voltage and current waveforms of the inverter. Since the grid voltage is a fundamental sinusoid waveform, the low order harmonics voltage caused by dead time effect can result in output current distortion and harmonics. The smaller LCL filter leads to a larger amplitude of harmonics current distortion. However, these output error voltage can be considered as a kind of disturbance caused by the dead time effect. Transforming the $\Delta u_{an}, \Delta u_{bn}, \Delta u_{cn}$ into dq-frame and moving the Δu_{dd} from the output of $G_d(s)$ to the input of $G_d(s)$, as shown in Fig. 2(a), the dead time effect disturbance in d-axis can be obtained as

$$d_{dtd}(s) = \frac{\Delta u_{dd}(s)}{G_d(s)} \tag{5}$$

It can be observed from Fig. 3 that the classical PI method in the application of LCL-type inverter shows weak attenuation ability at low-frequency band, for example only −10.36 dB for the dead time disturbance and −18.35 dB for the grid voltage harmonics disturbance at 300 Hz. Consequently, the PI approach cannot completely eradicate the negative effect of the ac-component periodic disturbances in LCL-type inverter. In the scenario, the grid voltage distortion and dead-time effect disturbances can lead to low-order harmonics at the inverter output current. Thus, if the controller is not well designed, the output current of the inverter does not meet the relative standard requirements.

3. Disturbance observer based current loop control

In order to prevent the negative effect of the grid voltage distortion, the dead time effect, and the parameter mismatches from the degradation of the output current quality in LCL-type inverter, this paper

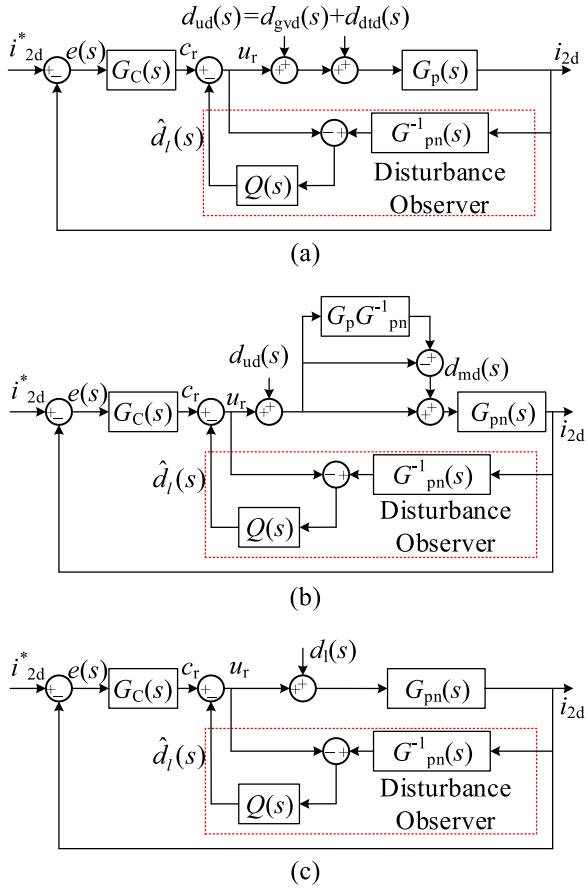

Fig. 4. Current loop control block of LCL-type inverter with disturbance observer: (a) Block diagram of the conventional disturbance observer; (b) Equivalent block diagram of conventional disturbance observer by normalizing the real plant; (c) Final equivalent block diagram of conventional disturbance observer.

proposes a disturbance observer based control method for three-phase LCL-type inverter as shown in Fig. 4. $G_{pn}(s)$ is the nominal LCL plant with appropriate active damping K_c considered. $Q(s)$ is the filter. $i^*_{2d}(s)$ is the inner loop reference current signal at d-axis. $d_{dtd}(s)$ and $d_{gvd}(s)$ are the voltage disturbances caused by the grid voltage distortion and the dead time effect, which can be aggregated as the voltage disturbance $d_{ud}(s)$ in the d-axis.

$$d_{ud}(s) = d_{dtd}(s) + d_{gvd}(s) \tag{6}$$

$d_{md}(s)$ is the model uncertainty disturbance caused by the parameter deviation and coupling effect. $\hat{d}_l(s)$ is the estimated lumped disturbance by disturbance observer. Then, as shown in Fig. 4(b), $d_{md}(s)$ can be expressed as

$$d_{md}(s) = [G_p(s)G^{-1}_{pn}(s) - 1][u_r(s) + d_{dtd}(s) + d_{gvd}(s)] \tag{7}$$

Then, $d_{dtd}(s)$, $d_{gvd}(s)$ and $d_{md}(s)$ can be aggregated as the lumped disturbances $d_l(s)$.

$$d_l = d_{dtd}(s) + d_{gvd}(s) + d_{md}(s) \tag{8}$$

It can be seen from Fig. 4(c) that the estimated lumped disturbance can be expressed as

$$\hat{d}_l(s) = Q(s)d_l(s) \tag{9}$$

Then, as shown in Fig. 4(c), the output current $i_{2d}(s)$ is obtained as

$$i_{2d}(s) = G_{ii}(s)i^*_{2d}(s) + G_{di}(s)d_l(s) \tag{10}$$

where

$$G_{ii}(s) = G_cG_{pn}/(1 + G_cG_{pn}) \tag{11}$$

$$G_{di}(s) = (1 - Q)G_{pn}/(1 + G_cG_{pn}) \tag{12}$$

Defining $D_e(s)$ is the error between the actual lumped disturbance $d_l(s)$ and the estimated disturbance $\hat{d}_l(s)$, which can be expressed as

$$D_e(s) = d_l - \hat{d}_l(s) \tag{13}$$

Substitute (9) into (13) , and yields

$$D_e(s) = [1 - Q(s)]d_l(s) \tag{14}$$

According to the Final-value theorem, one obtains

$$\begin{aligned} D_e(\infty) &= \lim_{t\to\infty} D_e(t) = \lim_{s\to 0} sD_e(s) \\ &= \lim_{s\to 0}[1 - Q(s)]\lim_{s\to 0} sd_l(s) = \lim_{s\to 0}[1 - Q(s)]\lim_{t\to\infty} d_l(t) \end{aligned} \tag{15}$$

It can be observed from (15) that the disturbance rejection performance of disturbance observer is closely related to the design of filter $Q(s)$. In general, the lumped disturbance $d_l(s)$ is bounded, and the $Q(s)$ filter is designed to be low-pass filter. In the bandwidth of the filter, i.e., $Q(s) = 1$, the lumped disturbance can be effectively estimated and compensated according to the final-value theorem. Therefore, the actual controlled plant is equivalent to the nominal one at low frequencies. Furthermore, considering that the inverse of the controlled plant is generally improper, the relative degree of $Q(s)$ should be guaranteed not less than that of $G_{pn}(s)$, which makes $Q(s)G^{-1}_{pn}(s)$ realizable.

However, it is important to note that the current distortion disturbance caused by the dead time effect and the grid voltage distortion is multi-frequencies ac-component disturbances. The lumped disturbances at inverter output current can be expressed as dc-component and ac-component periodic disturbances.

$$d_l(t) = \bar{d}(t) + \sum_{j=1}^{k} A_{mj}\sin(\omega_j t + \phi_j) \tag{16}$$

The first term on the right side of Eq. (16) is dc-component periodic disturbances, and the second term is a bounded ac-component periodic disturbances. According to the internal model principle, the periodic disturbances $d_l(s)$ can be completely estimated and compensated if the transfer function (12) in the DOB loop includes the model of that disturbance. The conventional simple low-pass filter $Q(s)$ in the DOB introduces phase lagging effect and cannot provide complete compensation for ac-component periodic disturbances, which are caused by the dead time effect and the grid voltage distortion. Therefore, a new DOB including the model of the ac-component periodic disturbances at the desired frequencies should be considered.

4. Proposed frequency adaptability fractional order harmonic disturbance observer

4.1. Frequency adaptability fractional order harmonic disturbance observer

To overcome the problem as mentioned in Section 3, the DOB should be designed to be effective against the low-order harmonic currents. According to the internal model principle, the model of the low-order current disturbances signal should be included in the DOB. For a sinusoidal signal, the model of sinusoidal signal is $G(s) = \omega/(s^2 + \omega^2)$. Then, one way to design DOB is to choose $Q(s)$ filter as $Q(s) = G(s) = \omega/(s^2 + \omega^2)$. However, if the disturbance signal contains multi-frequencies components, multiple internal models have to be set for each frequency signal, which results in the controller to be very complicated and is not suitable for engineering application. Thus, it is necessary to find a new internal model to describe multi-frequencies ac-component disturbance signals.

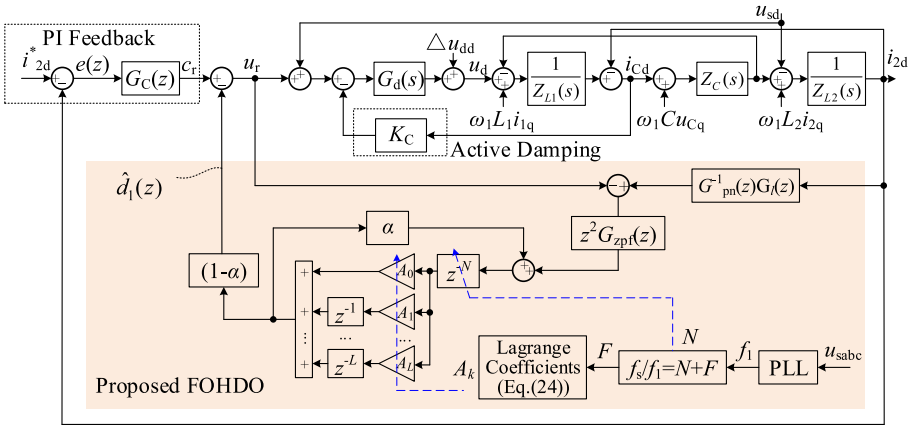

Fig. 5. Block diagram of LCL-type inverter system with frequency adaptability FOHDO based current controller in dq-frame.

The low-order harmonic current disturbance is periodic, that is, $d_l(s) = d_l(s)e^{-T_1 s} = d_l(s)e^{-NT_s s}$, where $1/T_1$ and $1/T_s$ are the fundamental frequency and the sampling frequency, or $d_l(z) = d_l(z)z^{-N}$, where $z = e^{j\Omega}$, $\Omega = \omega T_s \in [0, \pi]$, $N = int[f_s/f_1]$ is the integer sampling point in a fundamental period. Since the frequencies of $d_l(z)$ are known and contain dc-component disturbances, ac-component disturbances of grid fundamental frequency and their multiple, then its internal model $(1 - z^{-N})$ is also known. According to the internal model principle, it is known that the zeros of the transfer function $G_{di}(z)$ from the disturbances $d_l(z)$ to the inverter output current $i_{2d}(z)$ given by

$$i_{2d}(z) = G_{di}(z)d_l(z) = \frac{(1-Q)G_{pn}}{(1+G_c G_{pn})}d_l(z) \tag{17}$$

contain the roots of $d_l(z) = (1 - z^{-N})$, then the effect of the periodic disturbances $d_l(z)$ is eliminated on the inverter output current i_{2d} Jafari et al. (2015). In other words, this means that the internal model $(1 - e^{-T_1 s})$ or $(1 - z^{-N})$ should be included in the numerator of $(1 - Q)$ in Eq. (17). Therefore, this paper proposes an HDO design approach based on an infinite impulse response (IIR) filter to estimate and remove the periodic disturbance including the dead time effect, the grid voltage distortion and the parameter mismatches. The analysis is based on the z-domain for the purpose of digital implementation.

The transfer function of this IIR filter can be written in the following general form (Karaboga, 2009)

$$Q(z) = \frac{\sum_{i=0}^{J} b_i z^{-i}}{1 - \sum_{i=1}^{M} a_i z^{-i}} = \frac{X(z)}{1 - Y(z)} \tag{18}$$

where $M(\geq J)$ is the filter order, a_i and b_i are the filter coefficient. Hence, the design of this filter should consider the numerator of $(1-Q)$ containing the internal model $(1 - z^{-N})$, and satisfy

$$1 - Y(z) - X(z) = 1 - z^{-N} \tag{19}$$

Let $a_i = 0(i = 1, \ldots, N-1)$, and $a_N = \alpha$, $(0 < \alpha < 1)$ i.e. $Y(z) = \alpha z^{-N}$, and yields $X(z) = (1 - \alpha)z^{-N}$. Then, one can obtain as

$$Q(z) = (1 - \alpha)z^{-N}/(1 - \alpha z^{-N}) \tag{20}$$

It can be seen from Eqs. (17) and (20) that the numerator of the transfer function $G_{di}(z)$ in (17) contains the internal model of sinusoidal signal $(1 - z^{-N})$, which means that HDO can effectively estimate and suppress the low-order harmonics current. However, with the proposed Q filter, the HDO in Fig. 4 still has the following issues: (1) $G^{-1}_{P_n}(z)$ is improper and sensitive to the measurement noise; (2) Q filter needs sufficient attenuation ability at high frequencies to ensure the system stability; (3) To improve the stability of the HDO-based control system, time delay compensation should be considered (Baghaee et al., 2017; Wang et al., 2016); (4) Enhancing the frequency adaptability of the proposed HDO with a fixed sampling rate can perform high-quality disturbances suppression ability even in the presence of the grid frequency deviations.

For the first issue, a second-order low-pass filter $G_l(s)$ is introduced to make the $G^{-1}_{P_n}G_l$ proper and to decrease the gain of $G^{-1}_{P_n}$ in the high-frequency region.

$$G_l(s) = 1/(\tau s+1)^2 \tag{21}$$

where τ is the time constant of the second-order low pass filter.

For the second issue, a zero-phase low pass filter (ZPF) $G_{zpf}(z)$ can be introduced to the HDO. A general form of ZPF is

$$G_{zpf}(z) = h(0) + \sum_{n=1}^{m} h(n)(z^n + z^{-n}) \tag{22}$$

where m and $h(n)$ are the order and the coefficient of ZPF.

For the third issue, considering that the controlled plant $G_p(z)$ contains $1.5T_s$ delay time (Wang et al., 2016), 2 steps leading compensation z^2 is introduced into the output channel of HDO to compensate the time delay. The stability analysis with and without time delay compensation of the FOHDO can be seen in Fig. 10.

The ideal HDO can estimate and suppress any period harmonic disturbances. However, in a practical distribution network, the grid frequency f_1 is often time-varying in a certain range, e.g., due to uncertainties of the generation power and load. The performance of the proposed HDO may be degraded if the ratio f_s/f_1 is fractional.

To acquire the frequency adaptability of the proposed HDO method, the Lagrange interpolation polynomial Finite-impulse-response (FIR) filter was introduced in the proposed HDO loop. Assuming that $f_s/f_1 = N + F$, in which N is the integer part and $F(0 \leq F < 1)$ is the fractional order (FO) part, then the FO delay z^{-F} in the HDO can be approximated by a Lagrange interpolation polynomial as (Yang et al., 2016):

$$z^{-F} \approx \sum_{k=0}^{L} A_k z^{-k} \tag{23}$$

where L is the length of Lagrange-interpolation-based FIR filter, A_k is the Lagrange interpolation polynomial coefficient , and $k = 0, 1, 2, \ldots, L$. The coefficient A_k can be expressed as

$$A_k = \prod_{j=0, j\neq k}^{L} \frac{F-j}{k-j} \tag{24}$$

Specifically, if $L = 1$ in (24), (23) corresponds to a linear interpolation with $z^{-F} \approx (1 - F) + Fz^{-1}$. Considering the FO part z^{-F} and substituting (23) and (24) into (20) , the (20) is updated as

$$Q(z) = \frac{(1-\alpha)z^{-N}\sum_{k=0}^{L} A_k z^{-k}}{1 - \alpha z^{-N}\sum_{k=0}^{L} A_k z^{-k}} \tag{25}$$

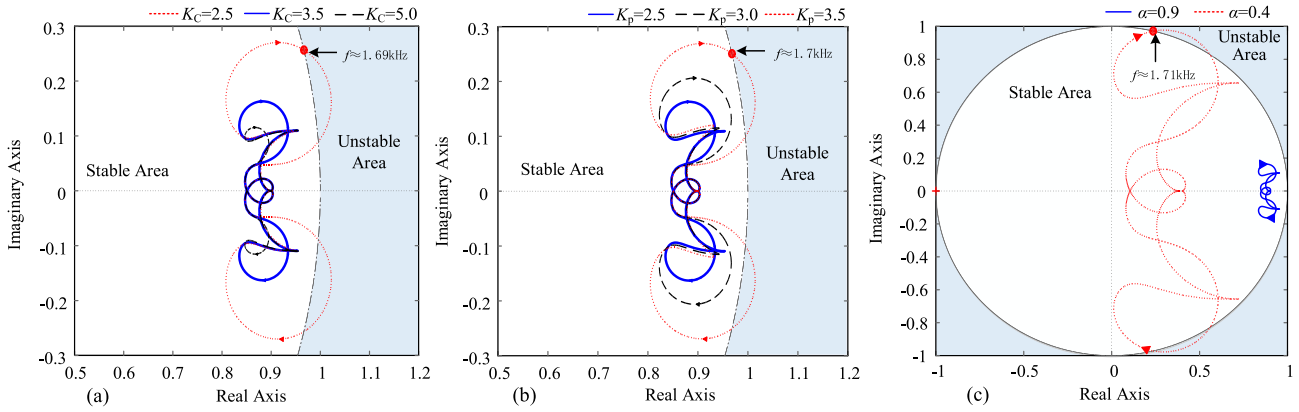

Fig. 6. Nyquist curve of $H(z)$ with different K_c, K_p and α value: (a) different K_c when K_p = 2.5 and α = 0.9; (b) different K_p when K_c = 3.5 and α = 0.9; (c) different α when K_p = 2.5 and K_c = 3.5.

Considering the four issues mentioned above, a block diagram of the proposed frequency adaptability FOHDO control for the three-phase LCL-type inverter system is shown in Fig. 5. The general approach of the proposed frequency adaptability FOHDO in Fig. 5 can suppress periodic (ac or dc) signals with arbitrary fundamental frequency. The periodic disturbances, which are mainly caused by the dead-time effect, the grid voltage distortion, the grid frequency deviation and the parameter mismatches, can be estimated and compensated to achieve high quality grid-connected currents. Moreover, the proposed FOHDO is located at the feedforward path for the current loop controller, which is different from the RC controller's feedback path. Therefore, a fast step response without distortion of the grid-connected currents can be obtained with the proposed FOHDO.

4.2. Stability and robustness analysis

Theorem 1. *For the FOHDO controlled system depicted in Fig. 5, the closed-loop system is stable if the following two conditions are satisfied:*

(i) $G_C(z)G_p(z)/(1+G_C(z)G_p(z))$ *is stable;*

(ii) $\|H(z)\|_\infty < 1$.

where

$$H = \alpha - \frac{(1-\alpha)G_{zpf}z^2(G_pG_{pn}^{-1}G_l - 1)}{1+G_CG_p} \tag{26}$$

Proof. The transfer function of the reference value $i_{2d}^*(z)$ and the voltage disturbance $d_{ud}(z)$ ($d_{ud}(z) = d_{dtd}(z) + d_{gvd}(z)$) to the output current $i_{2d}(z)$ in Fig. 5 can be obtained as

$$i_{2d}(z) = G_{ii}(z)i_{2d}^*(z) + G_{di}(z)d_{ud}(z) \tag{27}$$

where

$$G_{ii}(z) = \frac{1-\alpha z^{-N-F}}{1-z^{-N-F}H}\frac{G_cG_p}{1+G_cG_p} \tag{28}$$

$$G_{di}(z) = \frac{1-z^{-N-F}T}{1-z^{-N-F}H}\frac{G_p}{1+G_cG_p} \tag{29}$$

$$T(z) = \alpha + (1-\alpha)z^2G_{zpf} \tag{30}$$

In z-domain, the system is asymptotically stable if and only if all roots of (27) are in unity circle. Based on (27) and the small gain theorem (Hassan, 2002), the sufficient criterion of stability can also be expressed as $\|H(z)\|_\infty < 1$. Moreover, $G_C(z)G_p(z)/(1+G_C(z)G_p(z))$ must also be stable to stabilize the whole system; in other words, the closed-loop system must be stable before adding the FOHDO controller. ■

An example of a robust stability analysis is provided in Fig. 11.

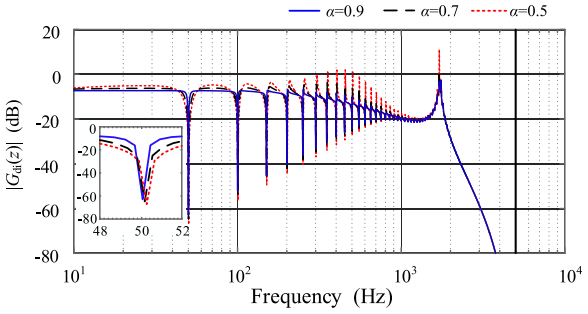

Fig. 7. Frequency characteristics of anti-disturbance of $G_{di}(z)$ with different α value.

Table 1
LCL-type inverter system parameters.

Symbol	Quantity	Value
u_{sa}	Grid voltage rms value	110 V
f_1	Fundamental frequency	50 Hz
u_{dc}	DC-link voltage	400 V
L_1	Inverter side inductor	1.0 mH
L_2	Grid side inductor	0.6 mH
C_f	Filter capacitor	20 μF
f_s/f_{sw}	Sampling freq./switching freq.	10 kHz

Remark 1. It can be seen from (29) that the harmonics disturbance can be effectively suppressed at frequencies due to $\{1-z^{-N-F}T(z)\} \approx 0$. Avoiding additional phase-lag in $T(z)$ introducing by G_{zpf}, G_{zpf} can be selected as a zero-phase low pass filter.

4.3. Parameters design and performance evaluation

The main parameters of the inverter system are shown in Table 1. The control parameters of the proposed FOHDO based control method in this paper include active damping K_c, PI controller G_c, FOHDO controller (including gain α, $G_l(z)$, $G_{zpf}(z)$ and L). Due to the high-order and the resonant characteristics of LCL-filter, which could increase the difficulty of designing FOHDO in LCL inverter application, the design details are presented as follows.

The capacitor current feedback active damping K_c is very effective and commonly used in engineering for LCL resonant suppression. The Nyquist curve of $H(z)$ with different K_c value is shown in Fig. 6(a). The active damping K_c can effectively suppress the resonant peak of LCL filter, and change the amplitude–frequency characteristics near the resonant frequency f_r. The larger K_c, the better damping effect for suppressing the resonant peak. However, due to the time delay in the digital controller, excessive active damping K_c reduces the stability

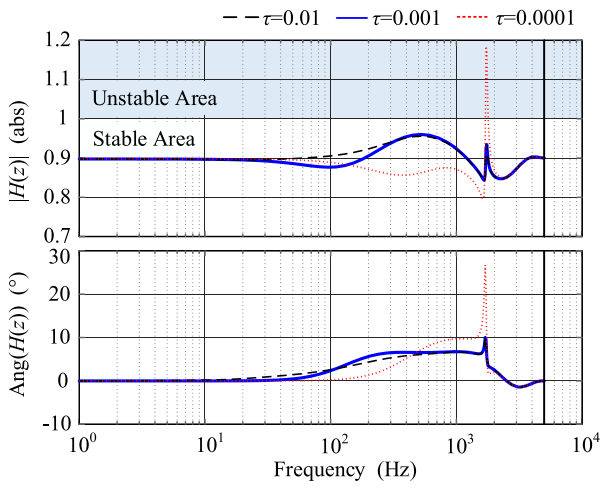

Fig. 8. Frequency characteristics of $H(z)$ with different time constant of the second-order low-pass filter $G_l(z)$.

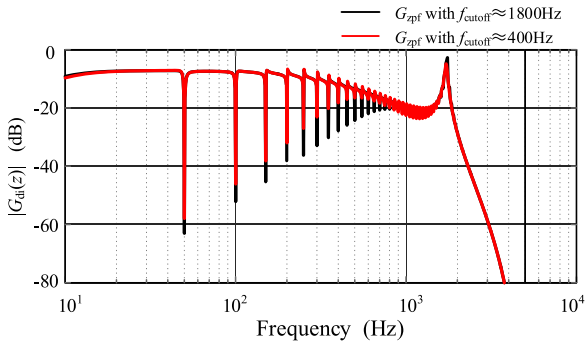

Fig. 9. Frequency characteristics of $G_{di}(z)$ with different cut-off frequency of ZPF.

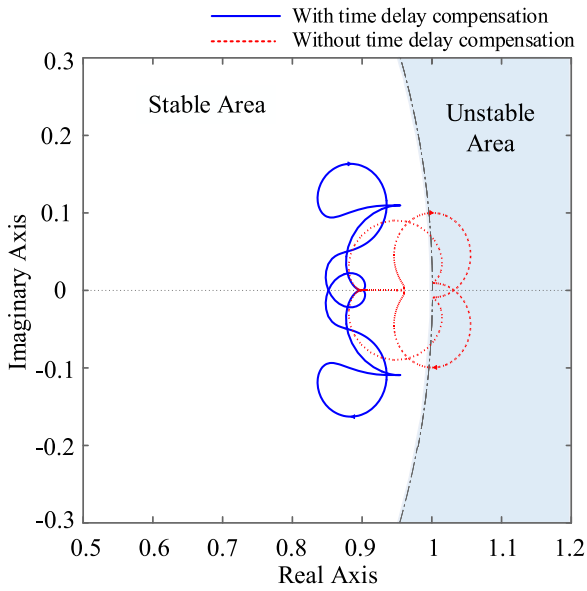

Fig. 10. Stability analysis with and without time-delay compensation of the proposed FOHDO.

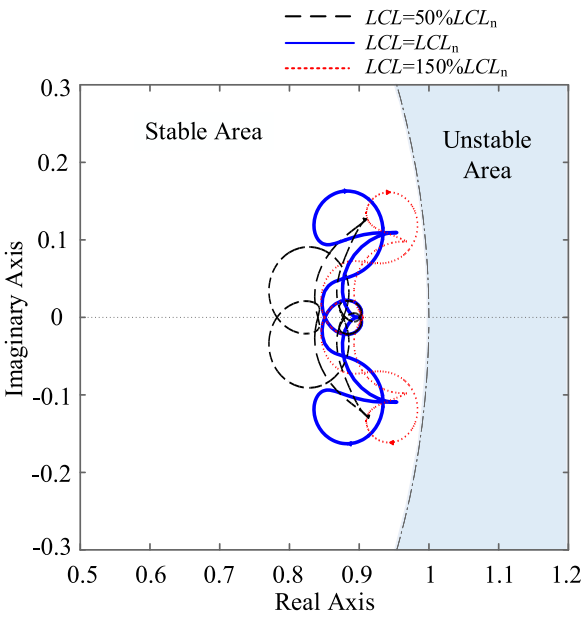

Fig. 11. Robustness analysis under the LCL filter parameter mismatches.

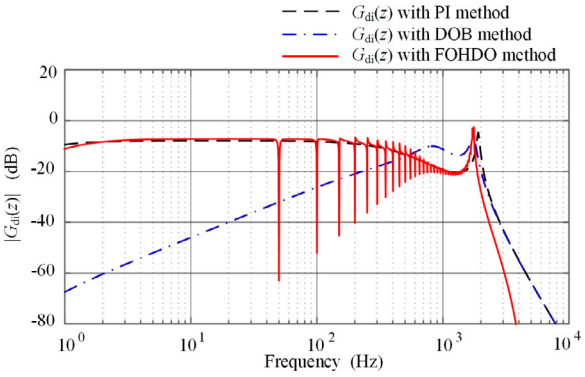

Fig. 12. Frequency characteristics of $G_{di}(z)$ with PI, DOB and FOHDO control for LCL-type inverter.

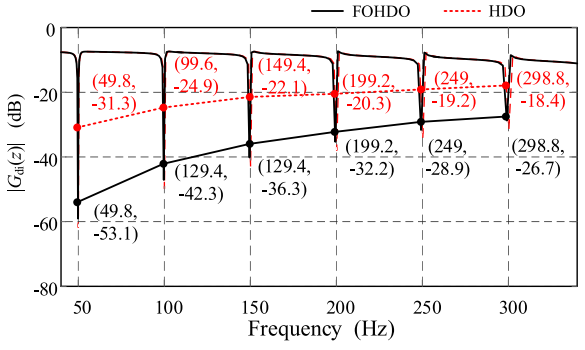

Fig. 13. Frequency characteristics of $G_{di}(z)$ with frequency deviation.

margin of the system (Ruan, 2018). Thus, $K_c = 3.5$ is chosen. Fig. 6(b) shows the Nyquist curve of $H(z)$ with different K_p value. The selection of G_c parameters should ensure that $G_p/(1 + G_cG_p)$ is stable; furthermore, since the HDO channel can be considered to be disconnected in the transient process, the dynamic performance is mainly determined by the PI controller. A larger K_p can improve the transient response; however, also decrease the stability margin of the controller. Then, $K_p = 2.5$ is chosen in this paper. The integral term K_i/s can be designed to have a negligible influence on system stability (Liserre et al., 2006), and $K_i = 10$ is chosen.

Fig. 7 shows the disturbance suppression performance of the FOHDO with different α. It can be observed that the proposed FOHDO

has much better harmonic disturbance suppression performance in harmonic frequencies. However, if α is chosen to be too small, the proposed FOHDO can be sensitive to frequency variation and degrade the disturbance rejection performance at the nominal frequency or even lead to unstable. The Nyquist curve of $H(z)$ in (26) is showed in Fig. 6(c). As it can be seen, the stability condition always meets due to $\|H\|_\infty < 1$ with $\alpha = 0.9$. If α is too small, such as $\alpha = 0.4$, the stability condition cannot be satisfied due to $\|H\|_\infty > 1$. Due to the high-order and resonant characteristics of LCL filter, the control parameters selection range is reduced. Therefore, α is chosen as 0.9 in this paper.

Because the inverse of the nominal controlled plant $G_{\mathrm{pn}}^{-1}(z)$ has high gain in the high frequencies, the stability margin of the system is reduced. Therefore, the second-order low-pass filter $G_{\mathrm{l}}(z)$ can be connected in series to provide high frequencies attenuation. Fig. 8 shows the frequency characteristics of $H(z)$ with different time constant τ of the second-order low-pass filter $G_{\mathrm{l}}(z)$. The too small time constant τ may amplify the resonant peak of LCL filter. Therefore, the time constant of $G_{\mathrm{l}}(z) = 1/(\tau s+1)^2$ is chosen to be 0.001. The inverse of the nominal controlled plant $G_{\mathrm{pn}}^{-1}(z)$ can be approximated as $1/s(L_1 + L_2)$. Then, the discrete transfer function $G_{\mathrm{l}}(z)G_{\mathrm{pn}}^{-1}(z)$ can be obtained as

$$\mathcal{Z}\left(G_{\mathrm{l}}(s)G_{\mathrm{pn}}^{-1}(s)\right) = \frac{0.07256z^2 - 0.07256}{z^2 - 1.81z + 0.8186} \tag{31}$$

The $G_{\mathrm{zpf}}(z)$ can increase the attenuation ability in high frequencies and enhance the robustness of the system. The higher order of $G_{\mathrm{zpf}}(z)$ is, the better effect of the filter, however, the design is more complicated. Fig. 9 shows the frequency characteristics of $G_{\mathrm{di}}(z)$ with different cut-off frequency of $G_{\mathrm{zpf}}(z)$. Smaller cut-off frequency of $G_{\mathrm{zpf}}(z)$ decreases the disturbances suppression ability of the proposed FOHDO method. In this paper, the cut-off frequency of $G_{\mathrm{zpf}}(z)$ is chosen as 1800 Hz, then $G_{\mathrm{zpf}}(z)$ can be expressed as

$$G_{\mathrm{zpf}}(z) = 0.25(z + 2 + z^{-1}) \tag{32}$$

Fig. 10 shows stability analysis with and without time-delay compensation of the proposed FOHDO. It can be seen that the FOHDO controlled system is unstable without time-delay compensation.

The stability analysis of the proposed FOHDO with the selected control parameters under parameter mismatches has been investigated, as shown in Fig. 11. The following two different parameter mismatches cases are studied: (1) The LCL filter parameters are 50% larger than the nominal values: $LCL = 150\%LCL_{\mathrm{n}}$ ($L_1 = 150\%L_{1\mathrm{n}}$, $C_{\mathrm{f}} = 150\%C_{\mathrm{fn}}$, $L_2 = 150\%L_{2\mathrm{n}}$); (2) The LCL filter parameters are 50% smaller than the nominal values: $LCL = 50\%LCL_{\mathrm{n}}$ ($L_1 = 50\%L_{1\mathrm{n}}$, $C_{\mathrm{f}} = 50\%C_{\mathrm{fn}}$, $L_2 = 50\%L_{2\mathrm{n}}$). It can be seen that the Nyquist curve of $H(z)$ always located within the unit circle, which means that the proposed method is robust to the LCL filter parameter mismatches.

The $G_{\mathrm{di}}(z)$ frequency characteristics with PI, DOB, and FOHDO control methods are illustrated in Fig. 12. It can be observed that the PI method has a poor ability to suppress the harmonic disturbance caused by the grid voltage distortion and the dead time effect. The dc and low-order frequency attenuation efficiency is enhanced by applying the DOB. However, the attenuation performance of DOB still needs to be improved at multiples of f_1, for example −18.1 dB at 300 Hz. Remember that, in practical power grids, low frequency and medium frequency disturbances still occur. On the contrary, it can be seen that the proposed FOHDO method outperforms with much smaller gain at each harmonic frequency compared to the conventional PI and DOB methods. Therefore, the proposed FOHDO method explicitly dramatically enhances the capacity for disturbances to reject multiples of f_1, indicating that the harmonic disturbances suppression performance has significantly enhanced by adopting the proposed FOHDO method.

Fig. 13 shows the magnitude–frequency response of anti-disturbance of $G_{\mathrm{di}}(z)$ when grid frequency deviates from nominal value 50 Hz to 49.8 Hz under a fixed sampling frequency of 10 kHz with and without considering fractional order part $F = 0.8$. It can be observed that

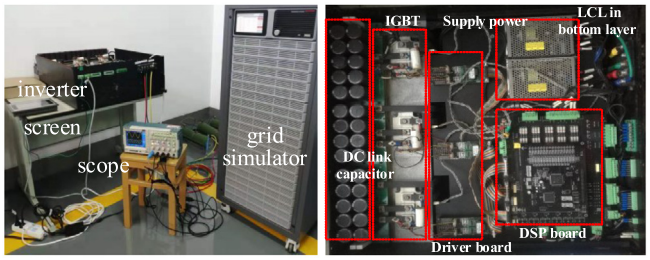

Fig. 14. Experimental setup of a three-phase three-wire inverter system.

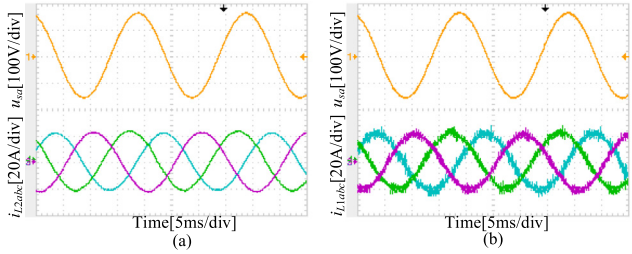

Fig. 15. Experimental result of the steady-state three-phase output current with $\alpha = 0.9$: (a) Grid-side current; (b) Inverter-side current.

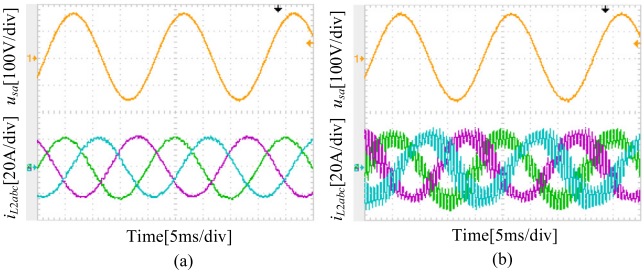

Fig. 16. Experimental results of grid-side current with different α in FOHDO: (a) $\alpha = 0.7$; (b) $\alpha = 0.5$.

the HDO method cannot exactly estimate and compensate low-order harmonic frequencies due to its not small enough attenuation gains for anti-disturbances. Therefore, HDO is sensitive to the grid frequency deviations. The FO delay z^{-F} can be well approximated by a Lagrange interpolation as shown in (23). In this paper, a linear interpolation is employed to enhance the frequency-deviation-immunity of the FOHDO as follows.

$$z^{-F} \approx (1 - F) + Fz^{-1} \tag{33}$$

The attenuation gains of FOHDO are retained small enough of the harmonic frequencies of interest. For instance, when the grid frequency deviates from nominal value 50 Hz to 49.8 Hz, the corresponding attenuation gain at the sixth-order harmonic frequency drops from −18.4 dB for the HDO to −26.7 dB for the FOHDO.

5. Experimental and simulation results

This section shows the experimental results based on a three-phase three-wire inverter prototype to verify the proposed FOHDO control method. The experimental setup consists of a three-phase LCL-type inverter, grid simulator, touchscreen interface and oscilloscope Tex 2024B, as shown in Fig. 14. The detailed experimental parameters are shown in Table 1. The simulation parameters are the same with that of the experiment. The THDs results were acquired by importing data of oscilloscope into Matlab. The Infineon IGBT module FF450R12KT4 and Concept driver 2SC0108T were configured to build the two-level

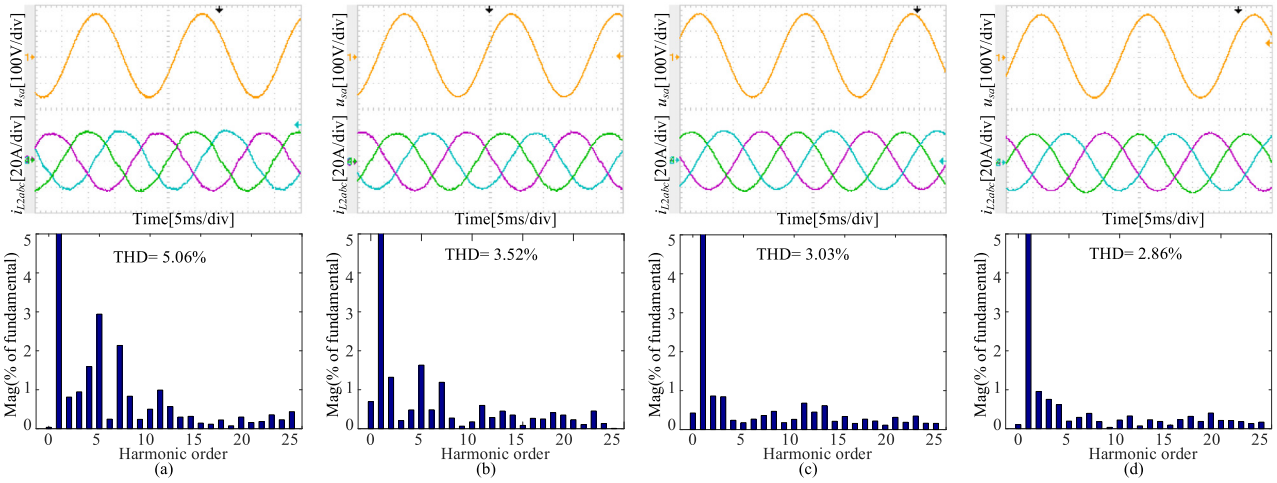

Fig. 17. Comparative experimental results with different control methods for three-phase LCL-type inverter with 4 μs dead time: (a) PI method; (b) DOB method; (c) PI–RC method; (d) Proposed FOHDO method.

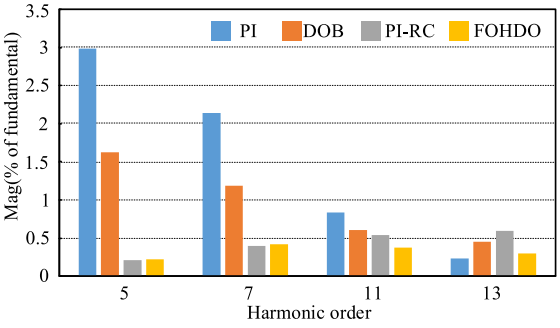

Fig. 18. The harmonic spectrum of the experimental results of the injected grid currents among the PI, DOB, PI–RC and the proposed FOHDO methods under 4 μs dead time.

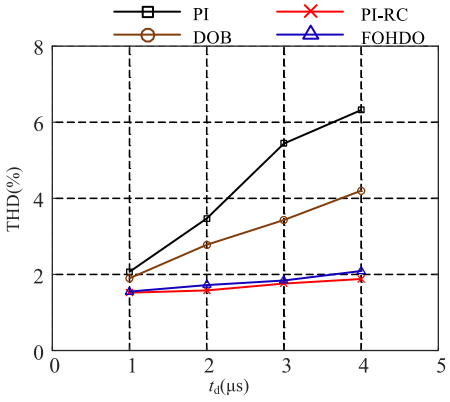

Fig. 19. Comparative simulation results of THDs of the output current with different control methods under different dead-time t_d.

three-phase three-wire LCL-type inverter. The experimental tests of the proposed FOHDO controller, DOB controller (Chen et al., 2016), PI–RC controller (Yang et al., 2018) and PI controller (Ruan, 2018) were carried out under various conditions. The detailed control parameters for the proposed FOHDO and PI controller in experiment are summarized as follows: $\alpha = 0.9$, $G_l(z) = 1/(0.001s+1)^2$, $G_{zpf}(z) = 0.25(z+2+z^{-1})$, $K_p = 2.5$, $K_c = 3.5$, $K_i = 10$. The RC harmonic compensator is expressed as

$$G_{RC}(z) = \frac{Q_{RC}(z)z^{-N}}{1 - Q_{RC}(z)z^{-N}} S(z) \tag{34}$$

where $Q_{RC}(z) = 0.97$ is chosen in the experiment, and $S(z) = k_{RC} z^m G_{LF}(z)$. The RC gain is designed as $k_{RC} = 1.4$ in terms of steady-state tracking error and stability. The phase-lead compensator m is determined in experimental tests and chosen as $m = 5$. $G_{LF}(z) = (0.1255z^2 + 0.251z + 0.1255)/(z^2 - 0.799z + 0.281)$ is a second-order low-pass filter to improve the controller robustness.

5.1. Case 1: Experimental results of steady-state and parameter tuning

Fig. 15 shows the steady-state grid-side and inverter-side currents under grid frequency of 50.0 Hz and dead time of $4\mu s$. The high frequencies switching current ripples are filtered out by LCL filter. Moreover, the interface shows that the output current is 15.0 A(rms) when the reference reactive current is set as 15 A, indicating that the proposed FOHDO method has an excellent steady-state tracking performance.

The experimental results of the grid-side current obtained by the proposed FOHDO controller with different α are shown in Fig. 16. It can be observed that the too small gain α of FOHDO leads to system instability, as shown in Fig. 16(b) with $\alpha = 0.5$.

5.2. Case 2: Experimental and simulation results under dead time effect

In order to verify the periodic disturbances suppression performance of the proposed FOHDO method, the dead time is set to be 4 μs in the experiment test, and the reference reactive output current of the inverter is set to $i_{2q}^* = 15 * 1.414$A. Fig. 17 show the comparative experimental results among the PI, DOB, PI–RC and the proposed FOHDO methods for LCL-type inverter. The harmonic spectrum of the injected grid currents shown in Fig. 17 is presented in Fig. 18. As shown in Fig. 17(a), having the dead time of 4 μs in the SPWM signal, due to the dead time effects, phase currents are distorted using the PI method. The phase current contains lots of lower-order harmonics, and the total harmonic distortion (THD) reaches 5.06%. Beneficial from DOB, the steady-state performance is improved and THD decreases to 3.53%. However, compared with the PI–RC and the proposed FOHDO, the conventional DOB scheme has a relatively poor performance on suppressing the harmonics disturbances, as shown the harmonic spectrum in Fig. 18, which means the weak ac-component periodic disturbances suppression ability of DOB. In comparison, the PI–RC method and the proposed FOHDO method can greatly remove the dead time effect. The THD of grid-side current with the PI–RC method is 3.11% as shown in Fig. 17(c). The THD of grid-side current with the FOHDO method is 2.86%, as shown in Fig. 17(d). Obviously, both PI–RC and

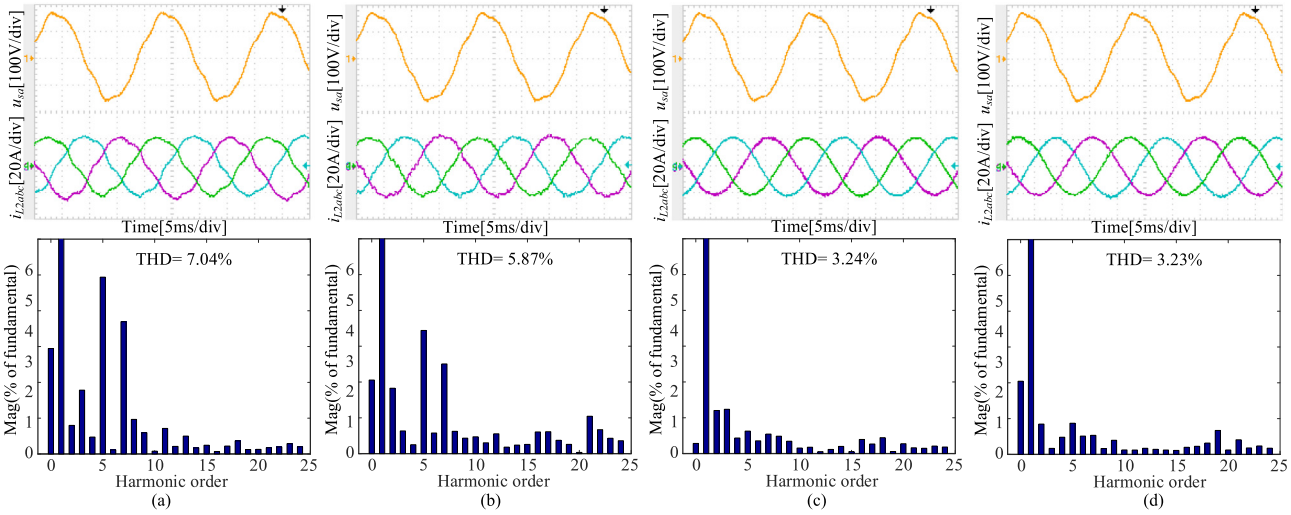

Fig. 20. Comparative experimental results with different control methods for three-phase LCL-type inverter under 0.05 pu 5th and 0.03 pu 7th harmonics of grid voltage: (a) PI method; (b) DOB method; (c) PI–RC method; (d) Proposed FOHDO method.

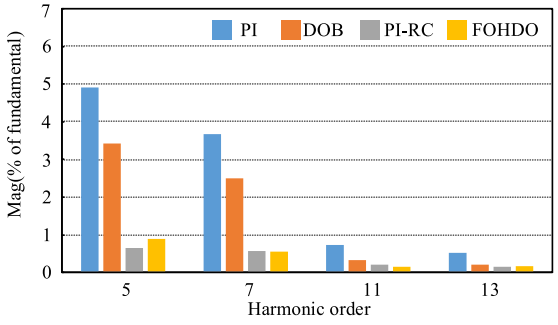

Fig. 21. The harmonic spectrum of the experimental results of the injected grid currents with different control methods under 0.05 pu 5th and 0.03 pu 7th harmonics of grid voltage.

FOHDO methods have a significant compensation performance against the dead time effect, which greatly reduce the THD of the inverter output current. The presented figures also indicate that the output current is about 15.0 A(rms) when the reference reactive current is set as 15 A(rms), which means that all of the four controllers can track the reference value without steady-state error. One could conclude that, compared with the PI and DOB methods, the proposed FOHDO method is able to effectively suppress ac-component periodic disturbances and attain good steady-state tracking performance.

Fig. 19 shows the comparative simulation results of THDs of the a-phase output current with different control methods under different dead-time t_d. In practical engineering, the dead time is always chosen as 2 μs ∼ 5 μs with f_{sw} = 10 kHz (Yang et al., 2018). It shows that as t_d increases, the harmonic content rises using PI and DOB methods, which means the weak ac-component periodic disturbances suppression ability of DOB. As expected, the simulation and experiment results are consistent and provide the essential evidence of strong ac-component periodic disturbances suppression ability with the proposed FOHDO to guarantee high-quality current even under ac-component periodic disturbances.

5.3. Case 3: Experimental results under grid voltage distortion

In order to verify the control performance of the proposed FOHDO under the grid voltage distortion, the grid voltage contains 0.05 pu 5th and 0.03 pu 7th harmonics, and the output current of the inverter is set to i_{2q}^{*} = 15 ∗ 1.414 A. Fig. 20 shows the comparative experimental results among the PI, DOB, PI–RC and the proposed FOHDO methods for three-phase LCL-type inverter under 0.05 pu 5th and 0.03 pu 7th harmonics of grid voltage. When the grid voltage distortion and the dead time effect are considered at the same time, the output current quality using the PI method has further deteriorated, and the THD reaches 7.04%, as shown in Fig. 20(a). The THD of grid-side current with the conventional DOB method is up to 5.87%, as shown in Fig. 20(b). In contrast, as shown in Fig. 20(c) and (d), both PI–RC and FOHDO methods show better grid voltage distortion rejection performance for LCL-type inverter. Under the grid voltage distortion, the THDs of the output current by PI–RC and FOHDO methods are 3.24% and 3.23%, respectively. Fig. 21 shows the harmonic spectrum of the experimental results of the injected grid currents with different control methods under 0.05 pu 5th and 0.03 pu 7th harmonics of grid voltage. It is in agreement with the conclusion that the proposed FOHDO method can suppress the injected grid current ac-component harmonics caused by the grid voltage distortion effectively.

Therefore, it can be concluded that the proposed FOHDO method has an excellent ac-component periodic disturbance rejection performance to eliminate the harmonic currents caused by the grid voltage distortion for LCL-type inverter.

5.4. Case 4: Experimental results under grid frequency deviation

The objective of this experiment is to investigate the effectiveness of the proposed frequency adaptability FOHDO method for LCL inverter system under variation of the grid frequency. The grid frequencies were programmed at 50.2 Hz and 49.8 Hz. If f_1 = 50.2 Hz, f_s/f_1 = 199.2 is fractional. If f_1 = 49.8 Hz, f_s/f_1 = 200.8 is also fractional. In these conditions, the harmonic disturbance performance of the proposed HDO is significantly degraded. Fig. 22 shows the comparative experimental results between the proposed HDO and FOHDO for three-phase LCL-type inverter with grid frequency ± 0.2 Hz deviation. It can be seen from Fig. 22(a) and (c) that the inverter output current is severely distorted (e.g., THD = 5.16% if f_1 = 50.2 Hz, and THD = 4.71% if f_1 = 49.8 Hz) without considering fractional order approximation for HDO method. In contrast, a linear interpolation to enhance the frequency adaptability of the proposed FOHDO was conducted. As a result, in the case of frequency deviations caused by the grid disturbances, it is indicated in Fig. 22(b) and (d) that the FOHDO produces excellent sinusoidal output current with very low THD (e.g., THD = 3.11% if f_1 = 50.2 Hz, and THD = 2.91% if f_1 = 49.8 Hz).

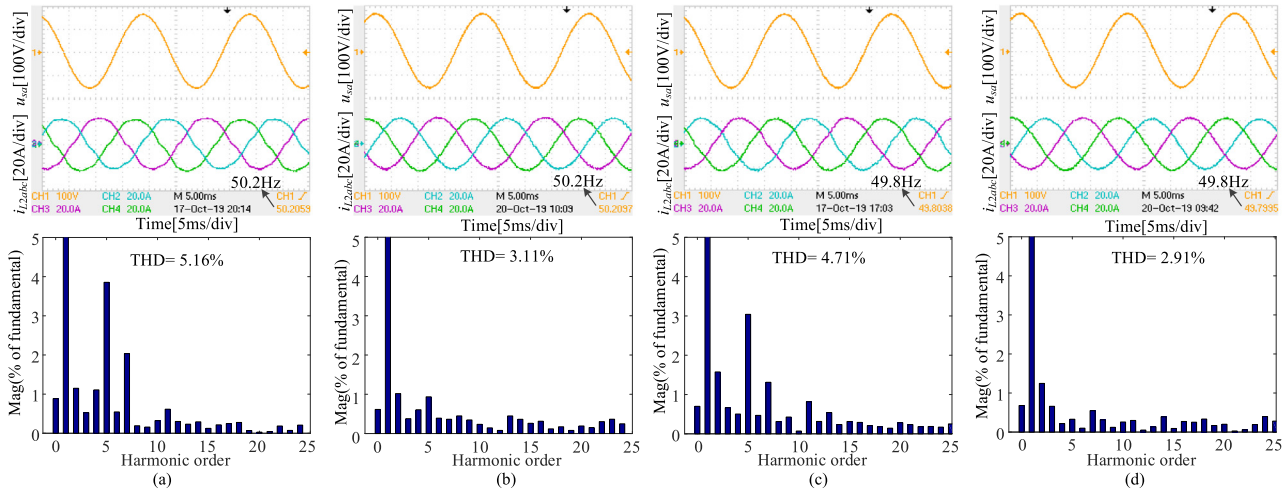

Fig. 22. Comparative experimental results between the proposed HDO and FOHDO methods for three-phase LCL-type inverter under grid frequency deviation: (a) HDO under grid frequency of 50.2 Hz; (b) FOHDO under grid frequency of 50.2 Hz; (c) HDO under grid frequency of 49.8 Hz; (d) FOHDO under grid frequency of 49.8 Hz.

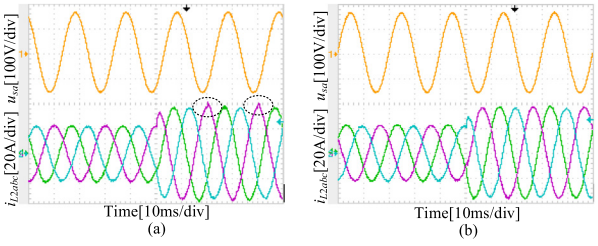

Fig. 23. Comparative experimental results of step-up transient performance: (a) PI–RC method; (b) FOHDO method.

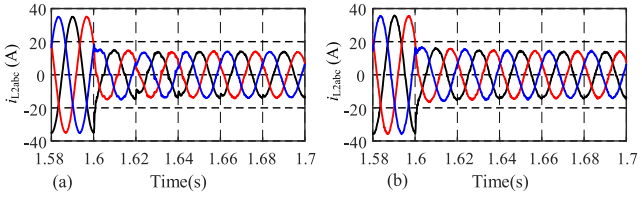

Fig. 24. Comparative simulation results of step-down transient performance: (a) PI–RC method; (b) FOHDO method.

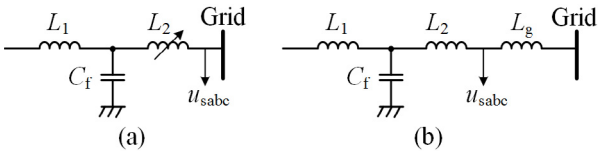

Fig. 25. Schematic diagram for testing the control performance of the parameter mismatches: (a) grid-side inductor parameter deviation $L_2 = 150\%L_{2n}$; (b) grid impedance deviation $L_g = 50\%L_{2n}$.

5.5. Case 5: Experimental and simulation results under transient response

This part is to test the transient performance for the proposed FOHDO. With considering the 4 μs dead time, the reference reactive current ($i^*_{2q} = 15 * 1.414$ A to $25 * 1.414$ A) step-up and ($i^*_{2q} = 25 * 1.414$ A to $10 * 1.414$ A) step-down response are carried out between the PI–RC and the proposed FOHDO. Figs. 23 and 24 show the comparative experiment and simulation results of step-up and step-down transient response performance between the PI–RC and the proposed FOHDO method, respectively. As shown in Figs. 23(b) and 24(b), the proposed FOHDO controller has a fast dynamic performance under the current reference step, and it can be found that the current flows smoothly without distortion during the transient response. The transient time is about 2 ms. The FOHDO feedforward channel can estimate and compensate the disturbance voltage caused by the dead time effect, while the feedback PI regulator guarantees the fast dynamic response. However, as shown in Figs. 23(a) and 24(a), the PI–RC method has a relatively poor transient response and current distortion performance compared with the proposed FOHDO method. The reason is that the RC channel is located at the feedback loop of the current controller while the FOHDO channel is located at the feedforward loop. There exists control coupling between PI and RC regulators at the feedback loop, which propagates the large error $e = i^*_{2q} - i_{2q}$ at step time into the next fundamental period and cause distortion of the inverter output current. Thus, the proposed FOHDO method is superior to the PI–RC method in terms of transient response.

5.6. Case 6: Experimental results under parameter mismatches

In order to verify the robustness of the proposed FOHDO against the parameter variation, two kinds of parameter mismatches, i.e., grid-side inductor parameter deviation $L_2 = 150\%L_{2n}$ and grid impedance deviation $L_g = 50\%L_{2n}$, were carried out as shown in Fig. 25. The dead time is maintained at 4 μs. Figs. 26 and 27 present the comparative experimental results for performance evaluation of PI, PI–RC and FOHDO under the grid-side inductor L_2 and the grid impedance L_g deviation, respectively. As can be seen from the experimental results, the three-phase output currents are well regulated with the PI–RC and the proposed FOHDO method. The experimental results demonstrate the ability of the proposed FOHDO to maintain the stability of LCL-type inverter system under the LCL filter and the grid impedance parameter mismatches.

5.7. Case 7: On-field test results

The on-field industry application is also considered, which is the motivation for us to explore high performance controller under complex real power grid operating conditions. The detailed parameters of 100 kVA three-phase four-wire LCL-type inverter system are shown as following: $L_1 = 0.2$ mH, $L_2 = 0.05$ mH, $C_f = 40$ μF, $f_s = 10$ kHz, $u_{sab} = 380$ V, $t_d = 4$ μs, IGBT FF450R12KT4 and Concept driver 2SC0108T. Fig. 28 shows the on-field results at 80 A (rms) load. The waveforms were recorded by Yokogawa DL750. The grid impedance L_g is unknown, and the THD of real power grid voltage is about

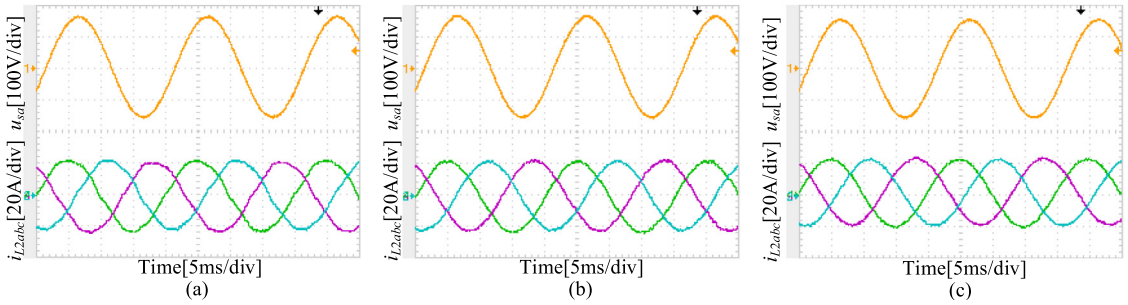

Fig. 26. Comparative experimental results of the control performance with different control methods when the actual inductance L_2 is changed to $L_2 = 150\%L_{2n}$: (a) PI method; (b) PI–RC method; (c) FOHDO method.

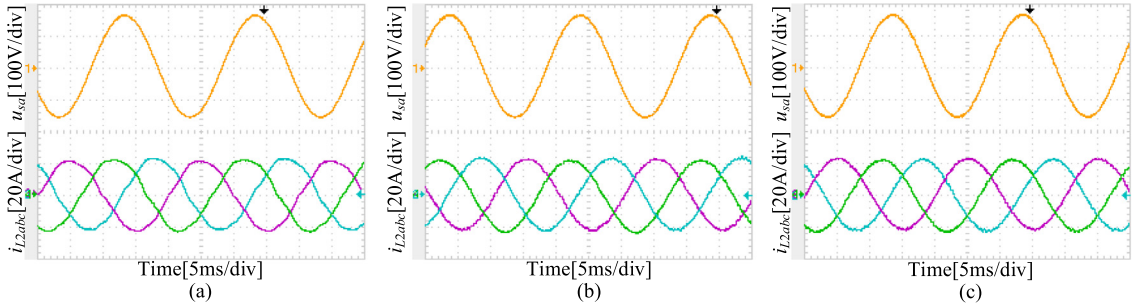

Fig. 27. Comparative experimental results of the control performance with different control methods when the actual grid inductance L_g is changed to $L_g = 50\%L_{2n}$: (a) PI method; (b) PI–RC method; (c) FOHDO method.

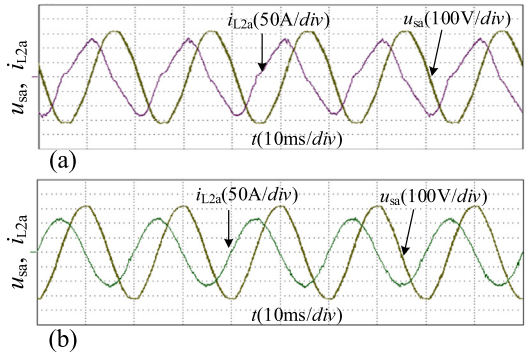

Fig. 28. Comparative on-field results at 80 A (rms) output current under real power grid: (a) PI method; (b) Proposed FOHDO method.

3.46%. Obviously, with the proposed FOHDO method, the output current harmonics are greatly reduced with the measured THD of 3.02%. Therefore, the proposed FOHDO method works well under on-field operating conditions.

6. Discussion

The detailed experimental and simulation results demonstrate that the proposed FOHDO method provides a good steady-state tracking accuracy and excellent ac-component periodic disturbances suppression ability under grid voltage distortion disturbances, dead time effect, and grid frequency deviation, as well as parameter mismatches conditions. Apart from the ac-component periodic disturbances suppression ability, it has fast dynamic response performance. Compared with the other applied methods such as PI and DOB methods, it is important to mention that the proposed FOHDO method explicitly enhances the ability to suppress ac-component periodic disturbances for LCL-type inverter. Moreover, compared with PI–RC method, the proposed FOHDO provides fast transient response without current distortion during step response. As a consequence, the proposed FOHDO approach is suitable for three-phase inverter system in terms of grid voltage distortion suppression, dead-time effect compensation, grid frequency variation adaptability and parametric uncertainties suppression.

It should be highlighted that the proposed FOHDO is suitable for both L- and LCL-type inverters. However, the high-order and the resonant characteristics of LCL-filter could affect the stability of the proposed FOHDO and narrow down the parameter's selection range.

7. Conclusion

This paper has presented the design and implementation of a novel FOHDO control solution to eliminate harmonic currents in the three-phase LCL-type inverter under nominal grid frequency and frequency deviation. The following conclusions can be made.

(1) The periodic disturbances, including the dead time effect, the grid voltage distortion, the grid frequency variation and the parameter mismatches, can cause significant distortion in the output current of the LCL-type inverter.

(2) The proposed FOHDO method for the LCL filter inverter can accurately estimate and eliminate the harmonic disturbances by embedding the internal model of periodic signals into the disturbance observer feedforward loop. Using the Lagrange interpolation to approximate fractional order delay in the HDO loop, the HDO has been transformed to FOHDO being of frequency adaptability, which improves control performance under the grid frequency variations.

(3) The stability analysis and the detailed parameters design guidelines of the proposed FOHDO for LCL-type inverter are given. The results show that the high-order and the resonant characteristics of LCL-filter affect the stability of the proposed FOHDO and narrow down the range of FOHDO control parameters.

(4) Compared with the PI, the conventional DOB and the PI–RC methods, the proposed FOHDO method shows the following features.

(i) The FOHDO method explicitly enhances the ability to suppress the multi-frequencies ac-component periodic disturbances for LCL-type inverter;

(ii) The FOHDO method can achieve zero steady-state tracking error and is robust to the parameter mismatches;
(iii) It has a quicker dynamic response performance without current distortion during step response;
(iv) The FOHDO method is capable of frequency adaptability.

(5) The effectiveness and superiority of the proposed FOHDO method have been verified by the experiment and simulation tests.

The proposed FOHDO offers a promising control strategy for a three-phase LCL-type inverter to improve output current quality.

Declaration of competing interest

The authors declare that they have no known competing financial interests or personal relationships that could have appeared to influence the work reported in this paper.

References

Baghaee, H. R., Mirsalim, M., Gharehpetian, G. B., & Talebi, H. A. (2017). A generalized descriptor-system robust h control of autonomous microgrids to improve small and large signal stability considering communication delays and load nonlinearities. *International Journal of Electrical Power & Energy Systems*, [ISSN: 0142-0615] *92*, 63–82. http://dx.doi.org/10.1016/j.ijepes.2017.04.007.

Blaabjerg, F., Pedersen, J. K., & Thoegersen, P. (1997). Improved modulation techniques for pwm-vsi drives. *IEEE Transactions on Industrial Electronics*, *44*(1), 87–95.

Blaabjerg, F., Teodorescu, R., Liserre, M., & Timbus, A. V. (2006). Overview of control and grid synchronization for distributed power generation systems. *IEEE Transactions on Industrial Electronics*, *53*(5), 1398–1409.

Blaabjerg, F., Zhe Chen, & Kjaer, S. B. (2004). Power electronics as efficient interface in dispersed power generation systems. *IEEE Transactions on Power Electronics*, *19*(5), 1184–1194.

Chen, L., & Peng, F. Z. (2008). Dead-time elimination for voltage source inverters. *IEEE Transactions on Power Electronics*, *23*(2), 574–580.

Chen, X., & Tomizuka, M. (2014). New repetitive control with improved steady-state performance and accelerated transient. *IEEE Transactions on Control Systems Technology.*, *22*(2), 664–675.

Chen, W., Yang, J., Guo, L., & Li, S. (2016). Disturbance-observer-based control and related methods—An overview. *IEEE Transactions on Industrial Electronics*, *63*(2), 1083–1095.

Chierchie, F., Paolini, E. E., & Stefanazzi, L. (2019). Dead-time distortion shaping. *IEEE Transactions on Power Electronics*, *34*(1), 53–63.

Cho, K., Kim, J., Choi, S. B., & Oh, S. (2015). A high-precision motion control based on a periodic adaptive disturbance observer in a pmlsm. *IEEE-ASME Transactions on Mechatronics*, *20*(5), 2158–2171.

Elkayam, M., Kolesnik, S., & Kuperman, A. (2019). Guidelines to classical frequency-domain disturbance observer redesign for enhanced rejection of periodic uncertainties and disturbances. *IEEE Transactions on Power Electronics*, *34*(4), 3986–3995.

Erika Twining, & Holmes, D. G. (2003). Grid current regulation of a three-phase voltage source inverter with an lcl input filter. *IEEE Transactions on Power Electronics*, *18*(3), 888–895.

Errouissi, R., & Al-Durra, A. (2018). Design of pi controller together with active damping for grid-tied lcl-filter systems using disturbance-observer-based control approach. *IEEE Transactions on Industry Applications*, *54*(4), 3820–3831.

Errouissi, R., & Al-Durra, A. (2019). Disturbance-observer-based control for dual-stage grid-tied photovoltaic system under unbalanced grid voltages. *IEEE Transactions on Industrial Electronics*, *66*(11), 8925–8936.

Hassan, K. (2002). *Nonlinear systems* (3rd ed.). Englewood Cliffs, NJ, USA: Prentice-Hall.

Jafari, S., Ioannou, P., Fitzpatrick, B., & Wang, Y. (2015). Robustness and performance of adaptive suppression of unknown periodic disturbances. *IEEE Transactions on Automatic Control*, *60*(8), 2166–2171.

Jiang You, M. V., & Ghasemi, N. (2018). Dc bus voltage stability improvement using disturbance observer feedforward control. *Control Engineering Practice*, *75*, 118–125.

Jiao, N., Wang, S., Liu, T., Wang, Y., & Chen, Z. (2019). Harmonic quantitative analysis for dead-time effects in spwm inverters. *IEEE Access*, *7*, 43143–43152.

Karaboga, N. (2009). A new design method based on artificial bee colony algorithm for digital iir filters. *Journal of the Franklin Institute*, [ISSN: 0016-0032] *346*(4), 328–348. http://dx.doi.org/10.1016/j.jfranklin.2008.11.003.

Li, W., Ruan, X., Pan, D., & Wang, X. (2013). Full-feedforward schemes of grid voltages for a three-phase LCL-type grid-connected inverter. *IEEE Transactions on Industrial Electronics*, *60*(6), 2237–2250.

Li, Y.-L., Sun, Y., & Dai, X. (2013). Robust control for an uncertain lcl resonant icpt system using lmi method. *Control Engineering Practice*, *21*(1), 31–41.

Liserre, M., Teodorescu, R., & Blaabjerg, F. (2006). Stability of photovoltaic and wind turbine grid-connected inverters for a large set of grid impedance values. *IEEE Transactions on Power Electronics*, *21*(1), 263–272.

Liu, J., Wu, W., Chung, H. S., & Blaabjerg, F. (2019). Disturbance observer-based adaptive current control with self-learning ability to improve the grid-injected current for LCL -filtered grid-connected inverter. *IEEE Access*, *7*, 105376–105390.

Muramatsu, H., & Katsura, S. (2018). An adaptive periodic-disturbance observer for periodic-disturbance suppression. *IEEE Transactions on Industrial Informatics*, *14*(10), 4446–4456.

Osório, C. R., Koch, G. G., Oliveira, R. C., & F., V. (2019). A practical design procedure for robust h2 controllers applied to grid-connected inverters. *Control Engineering Practice*, *92*, Article 104157.

Pan, D., Ruan, X., Bao, C., Li, W., & Wang, X. (2014). Capacitor-current-feedback active damping with reduced computation delay for improving robustness of lcl-type grid-connected inverter. *IEEE Transactions on Power Electronics*, *29*(7), 3414–3427.

Peña-Alzola, R., Liserre, M., Blaabjerg, F., Sebastián, R., Dannehl, J., & Fuchs, F. W. (2013). Analysis of the passive damping losses in lcl-filter-based grid converters. *IEEE Transactions on Power Electronics*, *28*(6), 2642–2646.

Ruan, X.-B. (2018). *Control techniques for lcl-type grid-connected inverters*. Springer Singapore.

Sun, K., Liu, L., Qiu, J., & Feng, G. (2020). Fuzzy adaptive finite-time fault-tolerant control for strict-feedback nonlinear systems. *IEEE Transactions on Fuzzy Systems*, in press.

Sun, G., & Ma, Z. (2017). Practical tracking control of linear motor with adaptive fractional order terminal sliding mode control. *IEEE-ASME Transactions on Mechatronics*, *22*(6), 2643–2653.

Sun, K., Qiu, J., Karimi, H. R., & Fu, Y. (2020). Event-triggered robust fuzzy adaptive finite-time control of nonlinear systems with prescribed performance. *IEEE Transactions on Fuzzy Systems*, in press.

Sun, K., Qiu, J., Karimi, H. R., & Gao, H. (2019). A novel finite-time control for nonstrict feedback saturated nonlinear systems with tracking error constraint. *IEEE Transactions on Systems, Man, and Cybernetics - Systems*, 1–12.

Sun, G., Wu, L., Kuang, Z., Ma, Z., & Liu, J. (2018). Practical tracking control of linear motor via fractional-order sliding mode. *Automatica*, *94*, 221–235. http://dx.doi.org/10.1016/j.automatica.2018.02.011.

Tang, Z., & Akin, B. (2017). Suppression of dead-time distortion through revised repetitive controller in pmsm drives. *IEEE Transactions on Energy Conversion*, *32*(3), 918–930.

Trivedi, A., & Singh, M. (2017). Repetitive controller for vsis in droop-based ac-microgrid. *IEEE Transactions on Power Electronics*, *32*(8), 6595–6604.

Wang, Y., Gao, Q., & Cai, X. (2011). Mixed pwm for dead-time elimination and compensation in a grid-tied inverter. *IEEE Transactions on Industrial Electronics*, *58*(10), 4797–4803.

Wang, M., Sun, J., & Chen, J. (2020). Stabilization of perturbed continuous-time systems using event-triggered model predictive control. *IEEE Transactions on Cybernetics*, 1–13.

Wang, J., Yan, J. D., Jiang, L., & Zou, J. (2016). Delay-dependent stability of single-loop controlled grid-connected inverters with LCL filters. *IEEE Transactions on Power Electronics*, *31*(1), 743–757.

Wu, Y., & Ye, Y. (2018). Internal model-based disturbance observer with application to cvcf pwm inverter. *IEEE Transactions on Industrial Electronics*, *65*(7), 5743–5753.

Yang, Y., Zhou, K., & Blaabjerg, F. (2016). Enhancing the frequency adaptability of periodic current controllers with a fixed sampling rate for grid-connected power converters. *IEEE Transactions on Power Electronics*, *31*(10), 7273–7285.

Yang, Y., Zhou, K., Wang, H., & Blaabjerg, F. (2018). Analysis and mitigation of dead-time harmonics in the single-phase full-bridge pwm converter with repetitive controllers. *IEEE Transactions on Industry Applications*, *54*(5), 5343–5354.

Yang, Y., Zhou, K., Wang, H., Blaabjerg, F., Wang, D., & Zhang, B. (2015). Frequency adaptive selective harmonic control for grid-connected inverters. *IEEE Transactions on Power Electronics*, *30*(7), 3912–3924.

Yin, Y., Liu, J., Sánchez, J. A., Wu, L., Vazquez, S., Leon, J. I., & Franquelo, L. G. (2019). Observer-based adaptive sliding mode control of NPC converters: An RBF neural network approach. *IEEE Transactions on Power Electronics*, *34*(4), 3831–3841.

Zhang, X., Wang, Y., & Yu, C. (2014). Mechanism of the control coupling and suppression strategy using pi and repetitive control in grid-connected inverters. *Proceedings of CSEE*, *34*(30), 5287–5295.

Zou, Z., Zhou, K., Wang, Z., & Cheng, M. (2014). Fractional-order repetitive control of programmable ac power sources. *IET Power Electronics*, *7*(2), 431–438.